Temperature-Dependent Structural Phase Transition in Rubrene Single Crystals: The Missing Piece from the Charge Mobility Puzzle?

Arie van Der Lee, Maurizio Polentarutti, Gilles Roche, Olivier Dautel, Guillaume Wantz, Frédéric Castet, Luca Muccioli

Temperature-dependent structural phase transition in rubrene single crystals: the missing piece from the charge mobility puzzle?

Arie van der Lee*[1], Maurizio Polentarutti[2], Gilles H. Roche[3,4], Olivier J. Dautel[3], Guillaume Wantz[4], Frédéric Castet[5], Luca Muccioli[6]

1. IEM, Université de Montpellier, CNRS, ENSCM, Montpellier, France; 2. Elettra, Sincrotrone Trieste S.C.p.A., Strada Statale 14 - km 163,5 in AREA Science Park, Basovizza, Trieste, 34149, Italy; 3. ICGM, Université de Montpellier, CNRS, ENSCM, Montpellier, France 4. Université de Bordeaux, IMS, CNRS, UMR 5218, Bordeaux INP, ENSCBP, 33405, Talence, 33405 ; 5. Université de Bordeaux, Institut des Sciences Moléculaires (UMR5255 CNRS), 351 cours de la Libération, F-33405, Talence, France, ; 6. Department of Industrial Chemistry, University of Bologna, 40136 Bologna, Italy
*email: arie.van-der-lee@umontpellier.fr

KEYWORDS (Word Style "BG_Keywords"). If you are submitting your paper to a journal that requires keywords, provide significant keywords to aid the reader in literature retrieval.

ABSTRACT: Accurate structural models for rubrene, the benchmark organic semiconductor, derived from synchrotron X-ray data in the temperature range 100-300 K show that its co-facially stacked tetracene backbone units remain blocked with respect to each other upon cooling down to 200 K and start to slip below that temperature. The release of the blocked slippage occurs at approximately the same temperature as the hole mobility crossover. The blocking between 200 and 300 K is caused by a negative correlation between the relatively small thermal expansion along the crystallographic *b*-axis and the relatively large widening of the angle between herringbone-stacked tetracene units. DFT calculations reveal that this blocked slippage is accompanied by a discontinuity in the variation with temperature of the electronic couplings associated to hole transport between cofacially-stacked tetracene backbones.

This manuscript has been accepted for publication in J. Phys. Chem. Lett. (2022). The final published version can be found here:

https://dx.doi.org/10.1021/acs.jpclett.1c03221

TOC graphic

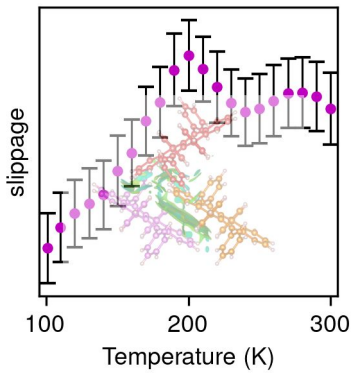

Rubrene, $C_{42}H_{28}$, is an organic semiconductor composed of a planar tetracene backbone with four symmetrically attached phenyl groups. It is considered as the benchmark compound in the field of single-crystal organic electronics. Various studies reported that this organic semiconductor has a high and reproducible hole mobility approaching 20 $cm^2V^{-1}s^{-1}$ when measured in field-effect transistors at room temperature.[1 2 3 4 5] As such, it is one of the major candidates for applications in field-effect transistors (FETs) and flexible organic opto-electronic devices.[6 7 8 9] The material is relatively easily fabricated at low cost and has in addition to the high carrier density a high photoluminescence yield, combined with strong visible light absorption.[10 11] The device performance of rubrene-based FETs was found to depend on different parameters, such as the layer thickness,[12] film oxidation,[13 14] and also temperature.[15 16 17 18] The carrier mobility was determined in the temperature range 100-300 K and found to display an abrupt decrease below 175-200K by a factor of 2.5 and 6 along the *a* and *b* axes of the unit cell along the *a* and *b* axes of the orthorhombic polymorph[19] with space group *Cmce*, as well as a vanishing of the mobility anisotropy along these two axes.[20 21]

An increase in mobility with decreasing temperature below ambient conditions was reported to occur for band-like transport organic semiconductors such as rubrene, PDIF-CN2, BTBT-C8, TMTSF, and TIPS-pentacene, but not in *e.g.* pentacene and sexithiophene.[22] In the former cases a characteristic temperature T^* was evidenced down to which the mobility increases with a power law $\mu \sim T^{-n}$ ($0.5 < n < 3$) before decreasing following an Arrhenius-type law at lower temperatures. In the case of rubrene, Frisbie *et al*. reported an exception for deuterium-substituted rubrene, albeit for only one of the three investigated samples.[23]

In an attempt to correlate the important mobility change in rubrene to a possible structural phase transition around 175 K, Jurchescu *et al*.[24, 25] determined the crystal structure at 25 K-spaced temperature intervals between 100 K and room temperature. They also performed a Differential Scanning Calometry (DSC) experiment and found a small exothermic process near 175 K associated with an enthalpy change of 3.13 kJ/mol. The analysis of the temperature-

dependent structural models did not give a clear indication for a structural transition around 175 K, and the authors concluded that the large change of the carrier mobility could not be fully explained from a re-arrangement of the intermolecular geometry. In a more recent study[26] using ultra-high resolution synchrotron data obtained at 20 and 100 K, the authors concluded that, at least between 20 and 100 K, π-π stacking interactions between cofacial tetracene units along the *b*-axis were unaltered and could consequently not explain any changes in the carrier mobility. An anomalous increase in the line width of certain low-frequency Raman peaks in the range 150–200 K was also reported and ascribed to an intermittent dynamic flipping of the side phenyl rings with different equilibrium positions at low and high temperatures.[27]

We propose here new temperature-dependent structural models derived from high-resolution synchrotron X-ray data measured between 100 and 300 K at 10 K-temperature intervals. These models show a weak but clear and reproducible transition within the 175-200 K temperature range. It is shown that down to ~190 K the tetracene backbones of cofacial rubrene molecules remain blocked with respect to each other, but start to slip below this temperature over a distance of approximately 0.02 Å down to 100 K. This slipping could explain the drastic drop in carrier mobility at low temperatures, as suggested by calculations of the electronic couplings J_i and the associated effective masses m_i^* between the co-facially π-stacked rubrene dimers.

The X-ray diffraction experiments were performed at the XRD1 beamline of Sincrotrone Elettra Trieste SCpA at a wavelength of 0.7000 Å in an open flow nitrogen cryostat between 100 K and 300 K. For each of the two selected crystals, full data were collected at 10 K steps for three complete consecutive cycles (up/down/up). All data sets were analyzed identically (see the Supporting Information (SI) for details) and showed no significant signs of X-ray radiation damage. Since the six different cycles yielded very similar results (see SI), we report here only the data obtained for one of the runs.

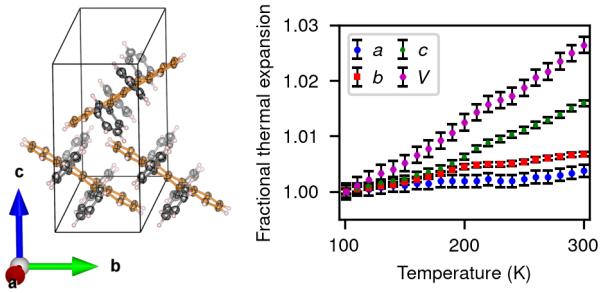

Fig. 1: Left: unit cell for the orthorhombic rubrene polymorph. The carbon atoms of the tetracene backbone are displayed in orange and those of the attached phenyl groups in grey. The size of thermal ellipsoid models is scaled at the 85% probability level. Right: Fractional thermal expansion along the three crystallographic axes and volumetric thermal expansion.

Fig. 1 shows the thermal expansion of rubrene along the three perpendicular axes as well as the resulting volumetric expansion. The linear thermal expansion coefficients are 15.2, 35.2, 82.5, and 133.8 MK^{-1} for *a*, *b*, *c* and the volume, respectively, which are not at all exceptional if compared to mean values reported for organic compounds: 71.4 MK^{-1} for the linear thermal expansion coefficient and 168.8 MK^{-1} for the volumetric one.[28] [29] However, both the thermal expansions along the *b* and *c*-axes and to a lesser extent the volume, show a change of slope near 190-200 K. The anisotropy of the thermal expansion reflects the anisotropic nature of the structure of rubrene, covalent and thus stiff intramolecular interactions mainly being present in the *ab*-plane.

The DSC measurements reported by Jurchescu *et al.*[24, 25] suggest that the transition associated with the drastic change of the mobility is first-order in nature, which would be compatible with the fact that no change of space group symmetry is detected. Our DSC measurements performed on 6 mg of freshly synthesized rubrene crystals did not show any exothermic peaks (Fig. S3). First-order phase transitions are usually accompanied by discontinuous changes of one or more cell parameters, which are not present here where only the first derivatives of the *b* and *c* parameters are discontinuous. This transition should thus rather be considered as a diffuse first-order type 0 structural phase transition[30] for which the discontinuities may be too small to be detected or simply too diffuse: Landau theory does not put a lower limit on the discontinuity expected for a first-order phase transition. [31] The structural changes are indeed very small (Fig. 2) which may explain the visual absence of any exothermal event in the DSC cycles.

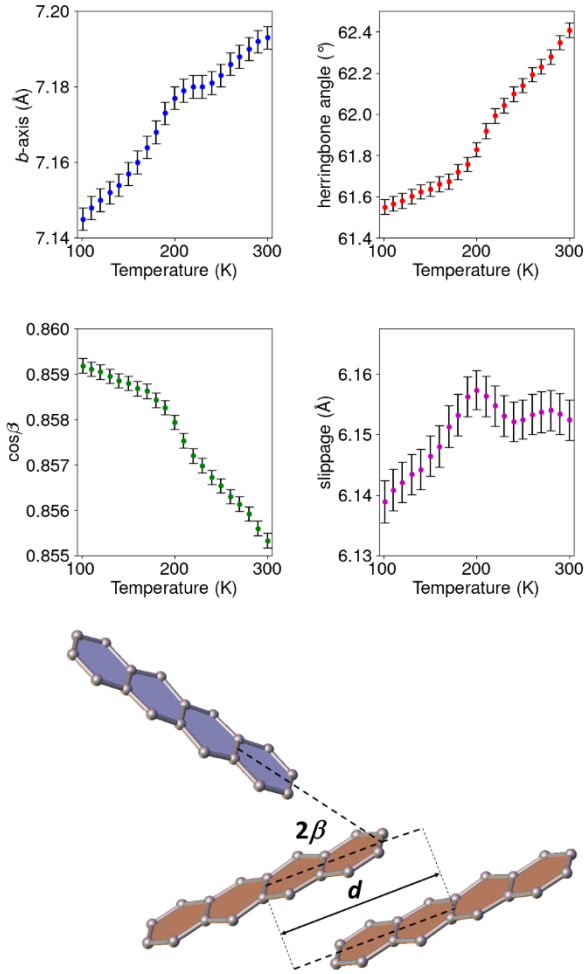

Fig. 2: Temperature evolution of the *b*-axis, the herringbone angle 2β, cos β, and the molecular slippage of two co-facial tetracene units. The error bars for the latter three quantities have been calculated from the least-squares standard uncertainties obtained for the *b*-axis values and the atomic coordinates using Monte-Carlo simulations (see SI, Fig. S4).

For analyzing in detail the structural changes as a function of temperature, we have quantified the molecular overlap between cofacial tetracene backbones using the same molecular displacement parameter $d = b.\cos\beta$ as defined by Jurchescu *et al.*[24], where β is the angle between the long axis of the tetracene unit and the *b*-axis. Rubrene packs according to the pitched π-stacking mode,[32] which maximizes the co-facial orbital overlap and which is responsible for the observed large mobility.[10] Although the packing of rubrene is not *stricto sensu* herringbone-like, for simplicity we refer to the angle between the two least-squares planes calculated from the positions of the carbon atoms constituting the two tilted tetracene units as the herringbone angle (Fig. 1). A simple inspection of the structure packing leads to the conclusion that β is half this herringbone angle, which is the angle between the long axis of the tetracene units adjacent in the *c* direction that, unlike along *b*, they are indeed not co-facial, but tilted by approximately 61°.

Fig. 2 shows the temperature evolution of *b*, β, cos β, and the slippage. Whereas the slope of *d* becomes smaller beyond 200 K, that of the herringbone angle becomes larger starting at 180-190 K. The result is that no relative slipping is observed anymore above this temperature. We have been able to observe this effect because of a finer temperature sampling (10 K) than used in the Jurchescu study[24] (25 K) but also because of the higher accuracy of the synchrotron data compared to the previous laboratory data. The analysis of the equivalent isotropic displacement parameters of the atoms constituting the phenyl side ring did not show much higher values in the 150-200 K range than outside this interval (Fig. S8), thus not supporting the intermittent disorder model of Ren *et al.*[27]

In an attempt of rationalizing and confirming these results in terms of molecular motions, we performed Molecular Dynamics simulations of a bulk rubrene crystal (see SI for details) using a classical force field already tested for rubrene[33] and a further refined version of it. Although failing in reproducing the discontinuities seen in Figs 1 and 2 – namely the slippage slight decreases with temperature in the calculations - both simulation series show an unprecedentedly reported nonlinear increase of *b* with temperature, thus substantiating the experimental findings.

The molecular slippage parameter is a one-dimensional geometric parameter, which may not reflect accurately the three-dimensional nature of the interaction region between two molecules. Therefore, this interaction volume was calculated using the Non-Covalent Interaction approach (NCI), which uses the promolecular density $\rho(\mathbf{r})$ for the determination of the reduced density gradient scalar field (RDG, $s(\rho)$).[34 35 36] The isosurfaces spanned by $s(\rho)$ expand over regions of space containing interacting atoms and molecules. Within this formalism, the second eigenvalue of the Hessian density matrix determines the attractive or repulsive nature of the interactions.

Fig. 3 gives the RDG for rubrene at 101 K and a three-dimensional view of the interaction regions between the molecules within the rubrene trimer, where the color scheme goes from blue for strong attractive interactions to red for strong repulsive interactions passing through green for weak Van der Waals type interactions. As expected, all intermolecular interactions are of the weak Van der Waals type, slightly attractive or repulsing, with the majority of interactions between the rubrene molecules with co-facial tetracene backbones. The interactions between the herringbone stacked molecules contribute greatly to the crystalline cohesion, although these interactions are not responsible for the mobility properties.

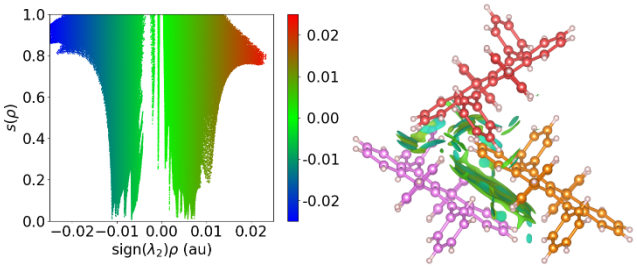

Fig. 3: Left: the reduced density gradient $s(\rho)$ versus $\text{sign}(\lambda_2)\rho$ for rubrene at 101 K. Right: NCI regions in rubrene trimer. The isosurface level of the RDG $s(\rho)$ is at 0.3. The color scheme is as in the left figure.

The NCI results can be interpreted semi-quantitatively by calculating the integrals of different moments of the electron density in the interaction volume, as well as the interaction volume Ω_a itself and the surface A_a of this volume. These parameters were determined for three different molecular configurations, the first consisting of a dimer of two rubrene molecules with co-facial tetracene backbones, the second of two adjacent rubrene molecules in herringbone stacking, and the third of a trimer of rubrene molecules with two co-facial tetracene units and a third one in herringbone stacking.

By comparing the values of the three different configurations (SI, Fig. S10), it can be estimated that the contribution to the crystal stability of the interactions between rubrene molecules with co-facial tetracene units is approximately twice as large as between herringbone stacked rubrene molecules. All subplots in Fig. 4 for the first configuration show discontinuties around 200 K, suggestive of a first order transition and most evident for the interaction surface A_a which decreases rapidly with temperature below 200 K and remains approximately constant above 200 K.

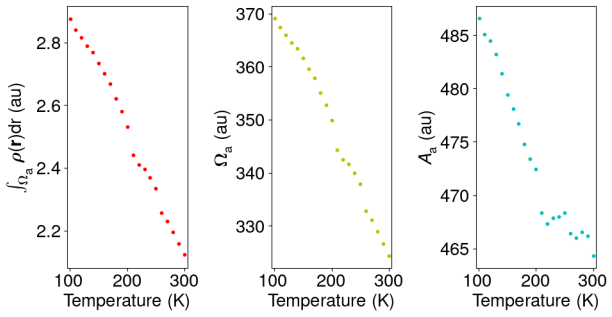

Fig. 4: NCI parameters as a function of temperature for a rubrene dimer with co-facial tetracene units: from the left to the right: integral of the electron density over the interaction volume, interaction volume, and interaction surface. All values are reported in atomic units.

Being in possession of accurate temperature-dependent measurements of the atomic coordinates in the crystal cell grants a unique opportunity of evaluating one fundamental ingredient for charge transport in rubrene, namely hole electronic couplings and the closely related electron masses. In fact, regardless and even before the choice of a charge transport model, for which there is no consensus in the literature for rubrene, the magnitude of electronic couplings should be assessed, and their variation with temperature could even determine a switch between one transport model to another. Therefore, the purpose of the following calculations is two-fold: obtaining physical insights on the effect of thermal expansion on the electronic couplings and providing essential information for further investigation of the charge transport mechanism in this system.

The electronic couplings (J) characterizing hole transfers between neighboring molecules were calculated using Density Functional Theory (DFT) at the B3LYP/6-31G(d) level, by employing the projection method involving the highest occupied molecular orbitals (HOMOs) of the monomers.[37] Fig 5 (left axis) shows the temperature evolution of the three most important transfer integrals. As reported in previous studies,[17 38 39 40] the largest coupling J_1 occurs between molecules stacked parallel to the b axis, *i.e.* once set the origin at one reference molecule, the second is found at positions $(0, \pm b, 0)$. A secondary but still sizable coupling J_2, about 6 times smaller than J_1, exists with molecules in the bc plane at positions $(0, \pm b/2, \pm c/2)$. Four weak interlayer couplings J_3 are provided by neighbors in positions $(\pm a/2, \pm b/2, 0)$ and even smaller ones from positions $(\pm a/2, 0, \pm c/2)$; the latter are reported only in the SI.

All couplings display a progressive decrease upon heating as a result of thermal expansion, which in turn stretches all intermolecular distances. One also notes that the trends for J_1 and J_2 show a change of slope between 175 and 200 K, in line with the temperature evolution of the b-axis. In addition, it can be observed neat correlation with the variation of the cosine of the herringbone angle in the whole temperature range (Figure 2), although one would expect the variation of J_1 to follow closely the variation of b instead, while for J_2 the relation with $\cos\beta$ could have been anticipated since larger herringbone angles correspond to less cofacial dimers.

Within a 1D band transport picture, charge carriers in the band can be described as particles with effective mass m^* inversely proportional to the intermolecular coupling: $m_i^* = \hbar^2/(2J_iL_i^2)$, with L_i the intermolecular distance along the coupling direction i, but in the case of rubrene only transport along the b direction can be treated as one-dimensional. The results for the effective mass calculations are shown in Fig. 5 (right axis). As expected, thermal expansion leads to an increase in effective mass with temperature, with m_1^* varying from 0.71 to 0.77. These values are consistent with previously reported temperature-dependent effective masses for rubrene computed from the dispersion of the valence band,[17] although the full temperature dependence was not reported in any previous study. It is interesting to note that, because of the factor L_i^2, the effective masses do not appear influenced by the structural phase transition and follow an approximate linear trend with temperature, suggesting that the effect of morphology changes on mobility could be

reflected to different extent depending on the transport mechanism, and foreseeing a stronger effect for hopping transport.

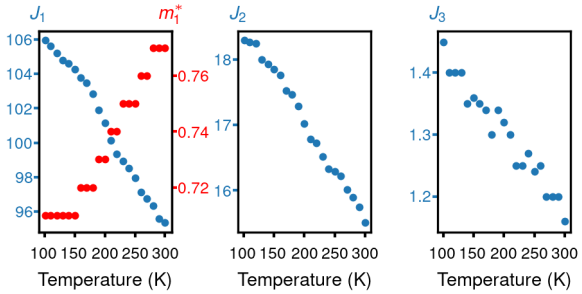

Fig. 5: Evolution of the electronic couplings J_i (in meV), and effective mass m_1^* along the *b* direction (in electron rest mass) as a function of temperature. Note the different scales used for J_1 and m_1.

Whilst it was recognized that the magnitude of the electronic couplings plays an important role in having band-like conducting behavior in an organic semiconductor, the cross-over from band-like to thermally activated mobility below *T** was not easily explained for intrinsic organic semiconductor materials, *i.e.* measured with air-gap dielectrics. Here we show that – at least in the case of non-deuterated rubrene – the release of the blocked slippage of the tetracene units below *T** may be linked to the mobility crossover.

Mei *et al.*[41] showed that crossovers from band-like to thermally activated charge transport could be achieved artificially by selecting a suitable dielectric material with a sufficiently large mismatch between its coefficient of thermal expansion and that of the organic semiconductor in the field-effect transistor, which was explained by the building up of strain-induced electronics traps during consecutive heating and cooling cycles. However, for rubrene a mobility crossover has been measured also with vacuum gate dielectrics and can thus not explain the crossover assuming externally induced strain. However, the anisotropic crystallographic thermal expansion of rubrene is similar to eigenstrain, which could have the same effects as an external mismatch strain. Indeed, with decreasing temperature the slippage parameter remains constant (Fig. 2) and thus the intermolecular arrangement unaltered, but below approximately 200 K an intermolecular rearrangement takes place which could lead to an increased hole trap density and a crossover to thermally activated charge carrier transport.

To further contextualize our results, it is worth acknowledging that, although the large electronic couplings in the *ab* plane suggest that hole transport in rubrene should be dominated by delocalized states, twenty years of research did not bring yet a consensus on the actual nature of this phenomenon and of its temperature dependence. The main obstacle to this objective is that most existing charge transport models[42 43 44 45 46 47] can reproduce in practice any experimental temperature behavior by the adjustment of some of their microscopic parameters (ionization potentials, electronic coupling and their static and dynamic fluctuations, electron-phonon couplings, …) which in turn are very challenging either to measure or calculate in the exact experimental conditions. Indeed, mobility measurements reflect a convolution of their temperature variation, but do not contain sufficient information to disentangle it.

The situation is further aggravated by the different length scale probed by the available measurements techniques, which can give rise to contrasting results,[48] and by the dominant role played by the substrate in determining the mobility temperature regime through electrostatic trapping, structural changes and thermal expansion.[49 50 51]

In this contribution, we provide an essential piece of information to the rubrene mobility puzzle, unequivocally showing that a structural transition occurs in rubrene single crystal in the 175-200 K temperature range, and how it affects some fundamental parameters used in charge transport theories. This finding is indirectly supported by past investigations and could lead to a partial reinterpretation and to a more complete understanding of charge transport in rubrene. Besides the already mentioned structural study of Jurchescu *et al.*[24, 25], hinting at a structural change at about 175 K, and the investigations by Podzorov and coworkers showing an abrupt decrease of mobility below 175-200 K,[20, 21] also the contact resistance for mobility measurement along the *b* axis was found to display a crossover between two different regimes, at approximately 175 K.[4] More recently, a similar crossover and a pseudo-band like temperature behavior at higher temperature, was reported also for the mobility along the *c* axis,[18] for which, owing to weak electronic couplings, one would expect instead hopping to be the dominant mechanism. In a further study along this line, Blülle *et al.* reported an abrupt change of mobility along *b*, between 185 and 200 K.[5]

The structural transition reported here provide thus a further possible interpretation key for existing literature results. We hope that this finding will trigger further experimental investigations on the temperature dependence of rubrene mobility and help achieving a full comprehension of its complex origin.

ASSOCIATED CONTENT

Supporting Information. Exprimental methods; full crystallographic data at www.ccdc.cam.ac.uk (2112501-2112626); crystallographic analyses for all runs; DSC curves; theoretical methods; python script for calculation of slippage parameter.

AUTHOR INFORMATION

Corresponding Author

Arie van der Lee - Institut Européen des Membranes, IEM - UMR 5635, ENSCM, CNRS, Université de Montpellier,

Montpellier, France; http://orcid.org/0000-0002-4567-1831; Email : arie.van-der-lee@umontpellier.fr.

Author Contributions

The manuscript was written through contributions of all authors.

Notes

The authors declare no competing financial interest.

ACKNOWLEDGMENT

Dan G. Dumitrescu is thanked for initiating the proposal for X-ray beamtime at the Elettra synchrotron, which was allocated under refererence 20200264. L.M. acknowledges funding from the MIUR-PRIN project "HARVEST" (protocol 201795SBA3). Computer time was provided by the Pôle Modélisation HPC facilities of the Institut des Sciences Moléculaires, co-funded by the Nouvelle Aquitaine region, as well as by the MCIA (Mésocentre de Calcul Intensif Aquitain) resources of Université de Bordeaux and of Université de Pau et des Pays de l'Adour. Grégory Excoffier (Spectropole, Marseille) from the French ЯÉCIPROCS network is thanked for carrying out additional X-ray measurements prior to the DSC analyses which have been performed by Joris Vezzani (University of Montpellier).

REFERENCES

(1) Sundar, V. C. Elastomeric Transistor Stamps: Reversible Probing of Charge Transport in Organic Crystals. *Science* **2004**, *303* (5664), 1644-1646. DOI: 10.1126/science.1094196.

(2) Takeya, J.; Yamagishi, M.; Tominari, Y.; Hirahara, R.; Nakazawa, Y.; Nishikawa, T.; Kawase, T.; Shimoda, T.; Ogawa, S. Very high-mobility organic single-crystal transistors with in-crystal conduction channels. *Applied Physics Letters* **2007**, *90* (10), 102120. DOI: 10.1063/1.2711393.

(3) Hasegawa, T.; Takeya, J. Organic field-effect transistors using single crystals. *Science and Technology of Advanced Materials* **2009**, *10* (2), 024314. DOI: 10.1088/1468-6996/10/2/024314.

(4) Menard, E.; Podzorov, V.; Hur, S. H.; Gaur, A.; Gershenson, M. E.; Rogers, J. A. High-Performance n- and p-Type Single-Crystal Organic Transistors with Free-Space Gate Dielectrics. *Advanced Materials* **2004**, *16* (23-24), 2097-2101. DOI: 10.1002/adma.200401017.

(5) Blülle, B.; Troisi, A.; Häusermann, R.; Batlogg, B. Charge transport perpendicular to the high mobility plane in organic crystals: Bandlike temperature dependence maintained despite hundredfold anisotropy. *Physical Review B* **2016**, *93* (3). DOI: 10.1103/physrevb.93.035205.

(6) Karak, S.; Lim, J. A.; Ferdous, S.; Duzhko, V. V.; Briseno, A. L. Photovoltaic Effect at the Schottky Interface with Organic Single Crystal Rubrene. *Advanced Functional Materials* **2013**, *24* (8), 1039-1046. DOI: 10.1002/adfm.201301891.

(7) Chang, Y.-T.; Liou, C.-C.; Su, J.-H. Investigation of Organic Optoelectronic Devices Doped with Different Rubrene Concentrations. *Materials Today: Proceedings* **2015**, *2* (1), 153-160. DOI: 10.1016/j.matpr.2015.04.016.

(8) Pei, K.; Wang, F.; Han, W.; Yang, S.; Liu, K.; Liu, K.; Li, H.; Zhai, T. Suppression of Persistent Photoconductivity of Rubrene Crystals using Gate-Tunable Rubrene/Bi 2 Se 3 Diodes with Photoinduced Negative Differential Resistance. *Small* **2020**, *16* (32), 2002312. DOI: 10.1002/smll.202002312.

(9) Liu, S.; Wu, H.; Zhang, X.; Hu, W. Research progress of rubrene as an excellent multifunctional organic semiconductor. *Frontiers of Physics* **2020**, *16* (1). DOI: 10.1007/s11467-020-0993-1.

(10) da Silva Filho, D. A.; Kim, E. G.; Brédas, J. L. Transport Properties in the Rubrene Crystal: Electronic Coupling and Vibrational Reorganization Energy. *Advanced Materials* **2005**, *17* (8), 1072-1076. DOI: 10.1002/adma.200401866.

(11) Irkhin, P.; Biaggio, I. Direct Imaging of Anisotropic Exciton Diffusion and Triplet Diffusion Length in Rubrene Single Crystals. *Physical Review Letters* **2011**, *107* (1). DOI: 10.1103/physrevlett.107.017402.

(12) Choi, J.-M.; Im, S. Optimum channel thickness of rubrene thin-film transistors. *Applied Physics Letters* **2008**, *93* (4), 043309. DOI: 10.1063/1.2966354 (acccessed 2021/11/10).

(13) Zhang, K. K.; Tan, K.; Zou, C.; Wikberg, M.; McNeil, L. E.; Mhaisalkar, S. G.; Kloc, C. Control of charge mobility in single-crystal rubrene through surface chemistry. *Organic Electronics* **2010**, *11* (12), 1928-1934. DOI: https://doi.org/10.1016/j.orgel.2010.08.019.

(14) Sinha, S.; Wang, C. H.; Mukherjee, M.; Mukherjee, T.; Yang, Y. W. Oxidation of Rubrene Thin Films: An Electronic Structure Study. *Langmuir* **2014**, *30* (51), 15433-15441. DOI: 10.1021/la503357t.

(15) Lin, K.-Y.; Wang, Y.-J.; Chen, K.-L.; Ho, C.-Y.; Yang, C.-C.; Shen, J.-L.; Chiu, K.-C. Role of molecular conformations in rubrene polycrystalline films growth from vacuum deposition at various substrate temperatures. *Scientific Reports* **2017**, *7* (1). DOI: 10.1038/srep40824.

(16) Okada, Y.; Uno, M.; Nakazawa, Y.; Sasai, K.; Matsukawa, K.; Yoshimura, M.; Kitaoka, Y.; Mori, Y.; Takeya, J. Low-temperature thermal conductivity of bulk and film-like rubrene single crystals. *Physical Review B* **2011**, *83* (11). DOI: 10.1103/physrevb.83.113305.

(17) Li, Y.; Coropceanu, V.; Brédas, J.-L. Thermal Narrowing of the Electronic Bandwidths in Organic Molecular Semiconductors: Impact of the Crystal Thermal Expansion. *The Journal of Physical Chemistry Letters* **2012**, *3* (22), 3325-3329. DOI: 10.1021/jz301575u.

(18) Pundsack, T. J.; Haugen, N. O.; Johnstone, L. R.; Daniel Frisbie, C.; Lidberg, R. L. Temperature dependent c-axis hole mobilities in rubrene single crystals determined by time-of-flight. *Applied Physics Letters* **2015**, *106* (11), 113301. DOI: 10.1063/1.4914975.

(19) Socci, J.; Salzillo, T.; Della Valle, R. G.; Venuti, E.; Brillante, A. Fast identification of rubrene polymorphs by lattice phonon Raman microscopy. *Solid State Sciences* **2017**, *71*, 146-151. DOI: https://doi.org/10.1016/j.solidstatesciences.2017.07.015.

(20) de Boer, R. W. I.; Gershenson, M. E.; Morpurgo, A. F.; Podzorov, V. Organic single-crystal field-effect transistors. *physica status solidi (a)* **2004**, *201* (6), 1302-1331. DOI: 10.1002/pssa.200404336.

(21) Podzorov, V.; Menard, E.; Borissov, A.; Kiryukhin, V.; Rogers, J. A.; Gershenson, M. E. Intrinsic Charge Transport on the Surface of Organic Semiconductors. *Physical Review Letters* **2004**, *93* (8). DOI: 10.1103/physrevlett.93.086602.

(22) Minder, N. A.; Ono, S.; Chen, Z.; Facchetti, A.; Morpurgo, A. F. Band-Like Electron Transport in Organic Transistors and Implication of the Molecular Structure for Performance Optimization. *Advanced Materials* **2011**, *24* (4), 503-508. DOI: 10.1002/adma.201103960.

(23) Xie, W.; McGarry, K. A.; Liu, F.; Wu, Y.; Ruden, P. P.; Douglas, C. J.; Frisbie, C. D. High-Mobility Transistors Based on Single Crystals of Isotopically Substituted Rubrene-d28. *The Journal of Physical Chemistry C* **2013**, *117* (22), 11522-11529. DOI: 10.1021/jp402250v.

(24) Jurchescu, O. D.; Meetsma, A.; Palstra, T. T. M. Low-temperature structure of rubrene single crystals grown by vapor transport. *Acta Crystallographica Section B Structural Science* **2006**, *62* (2), 330-334. DOI: 10.1107/s0108768106003053.

(25) Jurchescu, O. D. Low Temperature Crystal Structure of Rubrene Single Crystals Grown by Vapor Transport. Chapter 6 Groningen University, Groningen, 2006.

(26) Hathwar, V. R.; Sist, M.; Jørgensen, M. R. V.; Mamakhel, A. H.; Wang, X.; Hoffmann, C. M.; Sugimoto, K.; Overgaard, J.; Iversen, B. B. Quantitative analysis of intermolecular interactions in orthorhombic rubrene. *IUCrJ* **2015**, *2* (5), 563-574. DOI: 10.1107/s2052252515012130.

(27) Ren, Z. Q.; McNeil, L. E.; Liu, S.; Kloc, C. Molecular motion and mobility in an organic single crystal: Raman study and model. *Physical Review B* **2009**, *80* (24), 245211. DOI: 10.1103/PhysRevB.80.245211.

(28) Sun, C. C. Thermal Expansion of Organic Crystals and Precision of Calculated Crystal Density: A Survey of Cambridge Crystal Database. *Journal of Pharmaceutical Sciences* **2007**, *96* (5), 1043-1052. DOI: 10.1002/jps.20928.

(29) van der Lee, A.; Dumitrescu, D. G. Thermal expansion properties of organic crystals: a CSD study. *Chemical Science* **2021**, *12* (24), 8537-8547, 10.1039/D1SC01076J. DOI: 10.1039/D1SC01076J.

(30) Christy, A. G. Isosymmetric structural phase transitions: phenomenology and examples. *Acta Crystallographica Section B Structural Science* **1995**, *51* (5), 753-757. DOI: 10.1107/s0108768195001728.
(31) Swainson, I. P.; Hammond, R. P.; Cockcroft, J. K.; Weir, R. D. Apparently continuous isosymmetric transition in ammonium hexafluorophosphate ${\mathrm{NH}}_{4}{\mathrm{PF}}_{6}$. *Physical Review B* **2002**, *66* (17), 174109. DOI: 10.1103/PhysRevB.66.174109.
(32) Wang, C.; Hashizume, D.; Nakano, M.; Ogaki, T.; Takenaka, H.; Kawabata, K.; Takimiya, K. "Disrupt and induce" intermolecular interactions to rationally design organic semiconductor crystals: from herringbone to rubrene-like pitched π-stacking. *Chem Sci* **2020**, *11* (6), 1573-1580, 10.1039/C9SC05902D. DOI: 10.1039/C9SC05902D.
(33) Matta, M.; Pereira, M. J.; Gali, S. M.; Thuau, D.; Olivier, Y.; Briseno, A.; Dufour, I.; Ayela, C.; Wantz, G.; Muccioli, L. Unusual electromechanical response in rubrene single crystals. *Materials Horizons* **2018**, *5* (1), 41-50, 10.1039/C7MH00489C. DOI: 10.1039/C7MH00489C.
(34) Johnson, E. R.; Keinan, S.; Mori-Sánchez, P.; Contreras-García, J.; Cohen, A. J.; Yang, W. Revealing noncovalent interactions. *Journal of the American Chemical Society* **2010**, *132* (18), 6498-6506. DOI: 10.1021/ja100936w PubMed.
(35) Boto, R. A.; Contreras-García, J.; Tierny, J.; Piquemal, J.-P. Interpretation of the reduced density gradient. *Molecular Physics* **2016**, *114* (7-8), 1406-1414. DOI: 10.1080/00268976.2015.1123777.
(36) Boto, R. A.; Peccati, F.; Laplaza, R.; Quan, C.; Carbone, A.; Piquemal, J.-P.; Maday, Y.; Contreras-García, J. NCIPLOT4: Fast, Robust, and Quantitative Analysis of Noncovalent Interactions. *Journal of Chemical Theory and Computation* **2020**, *16* (7), 4150-4158. DOI: 10.1021/acs.jctc.0c00063.
(37) Valeev, E. F.; Coropceanu, V.; da Silva Filho, D. A.; Salman, S.; Brédas, J.-L. Effect of Electronic Polarization on Charge-Transport Parameters in Molecular Organic Semiconductors. *J Am Chem Soc* **2006**, *128* (30), 9882-9886. DOI: 10.1021/ja061827h.
(38) Stehr, V.; Pfister, J.; Fink, R. F.; Engels, B.; Deibel, C. First-principles calculations of anisotropic charge-carrier mobilities in organic semiconductor crystals. *Physical Review B* **2011**, *83* (15). DOI: 10.1103/physrevb.83.155208.
(39) Wen, S.-H.; Li, A.; Song, J.; Deng, W.-Q.; Han, K.-L.; Goddard, W. A. First-Principles Investigation of Anistropic Hole Mobilities in Organic Semiconductors. *The Journal of Physical Chemistry B* **2009**, *113* (26), 8813-8819. DOI: 10.1021/jp900512s.
(40) Gali, S. M.; Quarti, C.; Olivier, Y.; Cornil, J.; Truflandier, L.; Castet, F.; Muccioli, L.; Beljonne, D. Impact of structural anisotropy on electro-mechanical response in crystalline organic semiconductors. *Journal of Materials Chemistry C* **2019**, *7* (15), 4382-4391. DOI: 10.1039/c8tc06385k.
(41) Mei, Y.; Diemer, P. J.; Niazi, M. R.; Hallani, R. K.; Jarolimek, K.; Day, C. S.; Risko, C.; Anthony, J. E.; Amassian, A.; Jurchescu, O. D. Crossover from band-like to thermally activated charge transport in organic transistors due to strain-induced traps. *Proceedings of the National Academy of Sciences* **2017**, *114* (33), E6739-E6748. DOI: 10.1073/pnas.1705164114.
(42) Vehoff, T.; Baumeier, B.; Troisi, A.; Andrienko, D. Charge Transport in Organic Crystals: Role of Disorder and Topological Connectivity. *Journal of the American Chemical Society* **2010**, *132* (33), 11702-11708. DOI: 10.1021/ja104380c.
(43) Liu, C.; Huang, K.; Park, W.-T.; Li, M.; Yang, T.; Liu, X.; Liang, L.; Minari, T.; Noh, Y.-Y. A unified understanding of charge transport in organic semiconductors: the importance of attenuated delocalization for the carriers. *Materials Horizons* **2017**, *4* (4), 608-618, 10.1039/C7MH00091J. DOI: 10.1039/C7MH00091J.
(44) Giannini, S.; Carof, A.; Ellis, M.; Yang, H.; Ziogos, O. G.; Ghosh, S.; Blumberger, J. Quantum localization and delocalization of charge carriers in organic semiconducting crystals. *Nature Communications* **2019**, *10* (1), 3843. DOI: 10.1038/s41467-019-11775-9.
(45) Kunkel, C.; Margraf, J. T.; Chen, K.; Oberhofer, H.; Reuter, K. Active discovery of organic semiconductors. *Nature Communications* **2021**, *12* (1), 2422. DOI: 10.1038/s41467-021-22611-4.
(46) Girlando, A.; Grisanti, L.; Masino, M.; Bilotti, I.; Brillante, A.; Della Valle, R. G.; Venuti, E. Peierls and Holstein carrier-phonon coupling in crystalline rubrene. *Physical Review B* **2010**, *82* (3), 035208. DOI: 10.1103/PhysRevB.82.035208.
(47) Wang, L.; Beljonne, D. Flexible Surface Hopping Approach to Model the Crossover from Hopping to Band-like Transport in Organic Crystals. *The Journal of Physical Chemistry Letters* **2013**, *4* (11), 1888-1894. DOI: 10.1021/jz400871j.
(48) Tsutsui, Y.; Schweicher, G.; Chattopadhyay, B.; Sakurai, T.; Arlin, J.-B.; Ruzié, C.; Aliev, A.; Ciesielski, A.; Colella, S.; Kennedy, A. R.; et al. Unraveling Unprecedented Charge Carrier Mobility through Structure Property Relationship of Four Isomers of Didodecyl[1]benzothieno[3,2-b][1]benzothiophene. *Advanced Materials* **2016**, *28* (33), 7106-7114, https://doi.org/10.1002/adma.201601285. DOI: https://doi.org/10.1002/adma.201601285 (acccessed 2021/09/01).
(49) Podzorov, V.; Pudalov, V. M.; Gershenson, M. E. Field-effect transistors on rubrene single crystals with parylene gate insulator. *Applied Physics Letters* **2003**, *82* (11), 1739-1741. DOI: 10.1063/1.1560869 (acccessed 2021/09/01).
(50) Hulea, I. N.; Fratini, S.; Xie, H.; Mulder, C. L.; Iossad, N. N.; Rastelli, G.; Ciuchi, S.; Morpurgo, A. F. Tunable Fröhlich polarons in organic single-crystal transistors. *Nature Materials* **2006**, *5* (12), 982-986. DOI: 10.1038/nmat1774.
(51) Wu, Y.; Chew, A. R.; Rojas, G. A.; Sini, G.; Haugstad, G.; Belianinov, A.; Kalinin, S. V.; Li, H.; Risko, C.; Brédas, J.-L.; et al. Strain effects on the work function of an organic semiconductor. *Nature Communications* **2016**, *7* (1), 10270. DOI: 10.1038/ncomms10270.